

Test-Analysis Correlation of a Crash Simulation of a Vertical Drop Test of a Commuter-Class Aircraft

Karen E. Jackson and Edwin L. Fasanella
U.S. Army Research Laboratory, Vehicle Technology Directorate
NASA Langley Research Center
Hampton, VA

ABSTRACT

A finite element model of an ATR42-300 commuter-class aircraft was developed and a crash simulation was executed. Analytical predictions were correlated with data obtained from a 30-ft/s (9.14-m/s) vertical drop test of the aircraft. The purpose of the test was to evaluate the structural response of the aircraft when subjected to a severe, but survivable, impact. The aircraft was configured with seats, dummies, luggage, and other ballast. The wings were filled with 8,700 lb. (3,946 kg) of water to represent the fuel. The finite element model, which consisted of 57,643 nodes and 62,979 elements, was developed from direct measurements of the airframe geometry. The seats, dummies, luggage, simulated engines and fuel, and other ballast were represented using concentrated masses. The model was executed in LS-DYNA, a commercial finite element code for performing explicit transient dynamic simulations. Analytical predictions of structural deformation and selected time-history responses were correlated with experimental data from the drop test to validate the simulation.

INTRODUCTION

This paper describes the development and validation of a full-scale finite element model of an ATR42-300 commuter-class aircraft. The model was developed prior to the vertical drop test of the aircraft and analytical predictions were correlated with the experimental data. Model validations, such as described in this paper, are necessary to gain confidence in the application of explicit transient dynamic finite element codes for crashworthy design and certification. In fact, the “validation of numerical simulations” was identified as one of the five key technology shortfalls during the Workshop on Computational Methods for Crashworthiness that was held at NASA Langley Research Center in 1992 [1].

In 1998, the U.S. Army Research Laboratory Vehicle Technology Directorate (ARL-VTD) entered into an Inter-Agency Agreement (IAA) with the Federal Aviation Administration (FAA) William J. Hughes Technical Center for the purpose of validating crash simulations of airframe structures. As part of the IAA, finite element models were constructed of two 10-ft. (3.05-m) long Boeing 737 (B737) fuselage sections, one outfitted with an auxiliary fuel tank mounted beneath the floor and the other with two different overhead stowage bins and luggage. Vertical drop tests of these two fuselage sections were performed at the FAA Technical Center in 1999 and 2000, respectively [2, 3]. These tests provided a valuable opportunity to evaluate the capabilities of computational tools for crash simulation through test-analysis correlation. Full-scale three-dimensional finite element models of the B737 fuselage sections were developed using MSC.Dytran [4], a commercial explicit transient dynamic code, and simulations of the

vertical drop tests were executed. The model predictions were successfully validated through detailed test-analysis correlation, as documented in References 5 through 7.

In 2003, the IAA was extended for an additional five years, through 2008, and the model validation work entered a new phase with the development of a full-scale finite element model of the ATR42-300 aircraft. For this simulation, the model was developed using the pre-processing software package, MSC.Patran [8], and the final model was executed using another commercial code, LS-DYNA [9]. The FAA performed a 30-ft/s (9.14-m/s) vertical drop test of the aircraft to determine the impact responses of the airframe, floor, seat tracks, seats, dummies, and high-wing fuel system. Recently, the FAA has proposed dynamic performance criteria for seats in commuter aircraft that were based on empirical information obtained from prior airplane crash test data, which did not include airplanes representative in size of commuters. Consequently, this drop test was performed to provide impact data to evaluate the seat standards for this category of aircraft. The experimental program, model development, and test-analysis correlations are presented in subsequent sections of the paper.

EXPERIMENTAL PROGRAM

On July 30, 2003, a 30-ft/s (9.14-m/s) vertical drop test of an ATR42 aircraft was conducted by the FAA using the Dynamic Drop Test Facility located at the FAA Technical Center in Atlantic City, NJ. A pre-test photograph of the test article, raised to the drop height of 14 ft. (4.3 m), is shown in Figure 1. This twin-turboprop, high-wing, commuter-class aircraft was designed and manufactured through a joint effort by Aerospatiale in France and Aeritalia in Italy. The aircraft has a wingspan of 80 ft. (24.4 m), a seating capacity of 42-50 passengers, and a maximum gross take-off weight of approximately 36,800 lb. (16,693 kg). The drop test was performed onto a concrete surface. The purpose of the test was to evaluate the dynamic structural response of the aircraft when subjected to a severe, but survivable, impact. Particular attention was given to the seat and occupant responses to evaluate the FAA's proposed dynamic seat requirements for commuter-class aircraft.



Figure 1. Pre-test photograph of the ATR42 aircraft, raised to a drop height of 14 feet (4.3 m).

A schematic drawing of the floor of the aircraft is shown in Figure 2. The total weight of the fully loaded and instrumented aircraft was 33,200 lb. (15,060 kg). A large portion of the total weight was the 8,700-lb. (3,946 kg) of water added to the fuel tanks in the wing to represent fuel. In addition, 16 double-occupant aircraft seats weighing 54 lb. (24.5 kg) each and 3 single-occupant seats weighing approximately 20 lb. (9.07 kg) each were attached to seat tracks on the floor, as shown in Figure 2. Seven instrumented Anthropomorphic Test Dummies (ATDs) and 16 non-instrumented mannequins, each weighing 170 lb. (77.1 kg), were seated in various locations, as indicated in Figure 2. Ballast weights equaling 135- and 152-lb. (61.2- and 69.0-kg) were added to some of the empty seats to represent the mass of occupants. The forward and aft storage compartments were filled with 1,450- and 739-lb. (657.7- and 335.2-kg) of luggage, respectively. In addition to the ballast, two overhead stowage bins were mounted between Frame Section 30 (FS 30) and FS 34 on the right and left sides of the fuselage. The bins weighed 55 lb. (25.0 kg) each, 22-lb. (9.98 kg) empty weight plus 33-lb. (14.97 kg) ballast in each bin. Two cement-filled cylindrical drums were attached to the engine mounts on the wings, each weighing 1,290 lb. (585 kg), to represent the engines.

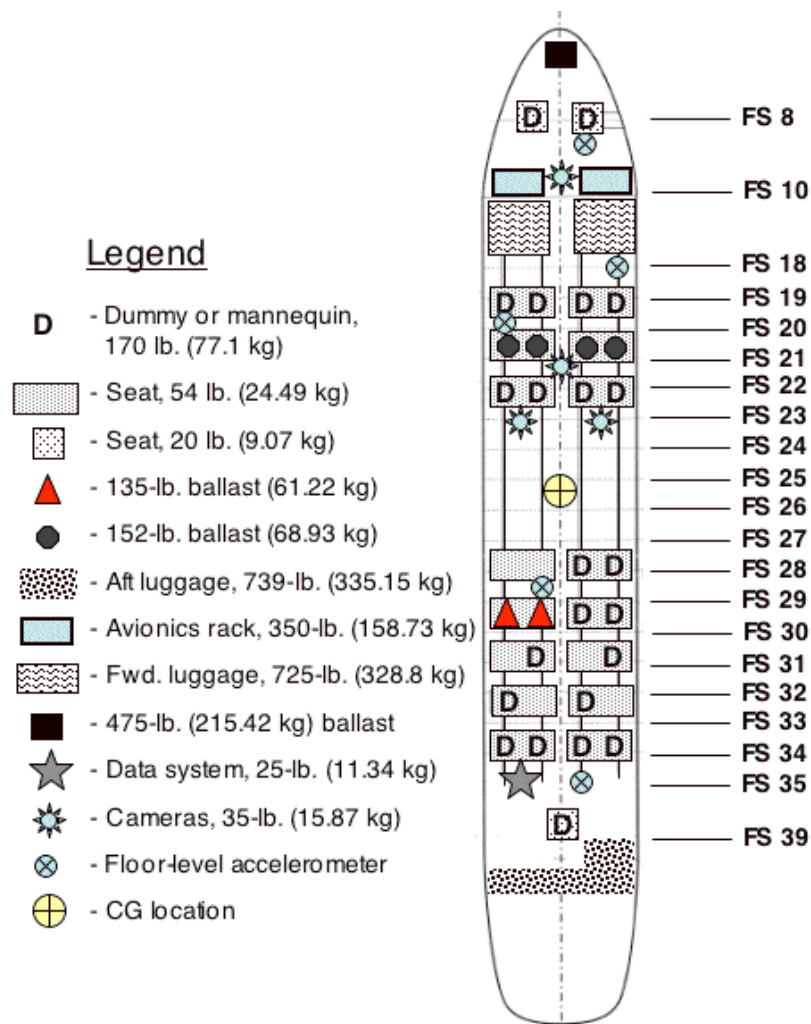


Figure 2. Floor schematic.

A dominant feature of this aircraft is the high wing, which is attached directly to heavy fuselage frames at FS 25 and FS 27 through four “dog bone” beams, as shown in Figure 3. The “dog bone” beams attach to brackets on the fuselage frames at a location approximately 60 in. above the floor. Four upper bracket assemblies are located on the top ends of these two fuselage frames. The measured longitudinal position of the center-of-gravity (CG) of the aircraft is approximately half way between FS 25 and FS 26, as shown in Figure 2. This measurement closely matches the CG location specified by the airframe manufacturer, as indicated in the Weight and Balance Manual [10].

The aircraft was instrumented with accelerometers, strain gages, load cells, pressure transducers, and string potentiometers. Test data were collected at 10,000 samples per second using two data acquisition systems, one on-board and one off-board. Of the channels available, eight acceleration responses were selected for correlation with the model. Of these eight responses, five were from accelerometers mounted on the floor of the fuselage cabin at locations shown in Figure 2. In addition, accelerometers located in the tail section at FS 47, the left sidewall at FS 18, and the center ceiling at FS 26 were also selected for comparison. These locations are not shown in Figure 2.

A post-test photograph showing an overall exterior view of the aircraft is shown in Figure 4. The primary damage mode to the airframe was the failure of the heavy fuselage frames supporting the wing at FS 25 and FS 27, causing the wing to subsequently displace through the fuselage cabin. The aluminum structure supporting the wing was crushed and fractured. A post-test photograph showing a close-up view of the wing/fuselage region is shown in Figure 5 (a). Further inspection of the airframe following the test indicated that several of the seats failed, as shown in Figure 5 (b).

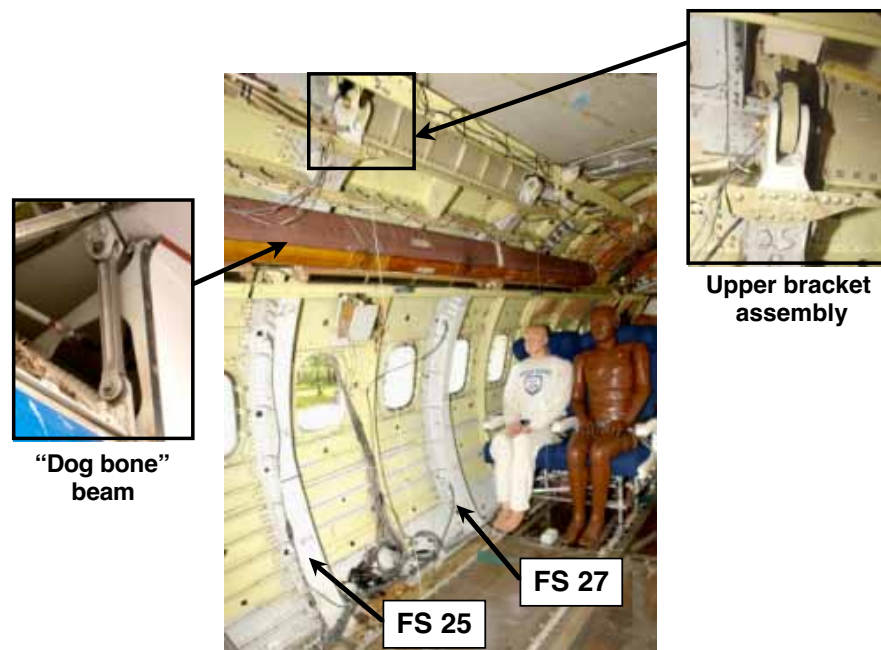


Figure 3. Photograph showing the aircraft interior at FS 25 and FS 27. Note that the locations of the “dog bone” beam and upper bracket assembly are highlighted.



Figure 4. Post-test photograph of the ATR42 aircraft showing an overall view.



(a) Close-up view.



(b) Interior view.

Figure 5. Post-test photographs.

MODEL DEVELOPMENT

The finite element model of the ATR42 aircraft was developed from direct measurements of the airframe geometry, which were input into MSC.Patran database files. When completed, the geometry model was discretized into a finite element mesh, element and material properties were assigned, contact and initial velocity conditions were defined, and the model was executed to generate analytical predictions of structural deformation and acceleration and velocity time-history responses. The finite element model of the ATR42 aircraft, shown in Figure 6, contained 57,643 nodes and 62,979 elements including 60,197 quadrilateral shell elements; 551 triangular shell elements; 526 beam elements; and, 1,705 point elements which were used to assign concentrated masses to nodes in the model. Additional information on the model development process can be found in Reference 11.

An automatic contact (CONTACT_AUTOMATIC_SINGLE_SURFACE) was specified for the model, which is a generic contact definition in LS-DYNA that prescribes that no node can penetrate through any surface in the model. An impact surface was created to represent the concrete pad beneath the drop tower. This surface was modeled as a 5-in. (0.127-m) thick aluminum plate, encompassing the total length and width of the aircraft, as shown in Figure 6(c). This representation did not match the impact surface used in the experiment; however, it was sufficient for the simulation. Four main material properties were defined in the model for

aluminum Al-2024-T3, aluminum Al-7075-T6, aluminum Al-7050-T7452, and titanium Ti-6Al-4V. The properties were defined using the MAT_PLASTIC_KINEMATIC card in LS-DYNA for a linear elastic-plastic material with input values for density, Poisson's ratio, Young's modulus, yield stress, hardening modulus, and an ultimate failure strain. The specific properties used in the model are shown in Table 1. Most of the sheet metal parts, such as the outer skin were assigned material properties of Al-2024-T3. The forged metal parts, such as the fuselage frames, floor beams, and seat tracks were assigned material properties of Al-7075-T6, except for the two heavy fuselage frames at FS 25 and FS 27 which were assigned properties of Al-7050-T7452. The "dog bone" beams used to attach the wing to the fuselage frames at FS 25 and FS 27 were assigned material properties of titanium Ti-6Al-4V. The material property designation and mass of each component were obtained from the aircraft manufacturer's Weight and Balance Manual [10] and the material property values were estimated based on values found in MIL-HDBK-5H [12].

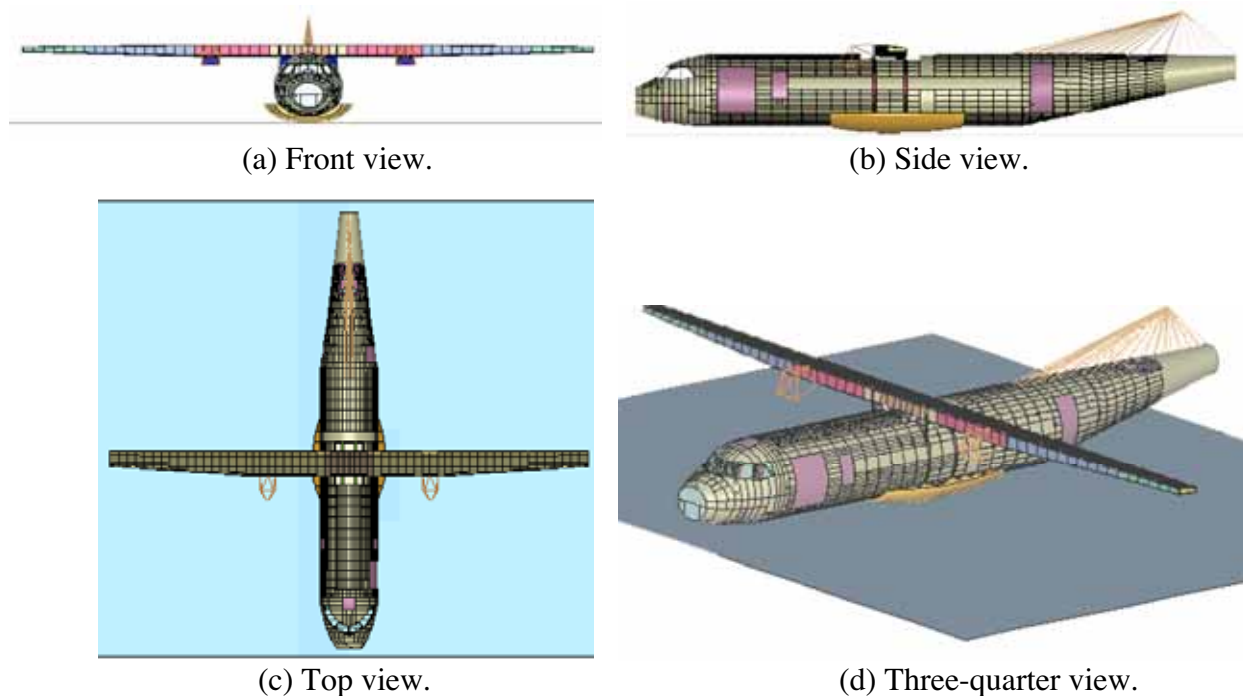


Figure 6. Finite element model of the ATR42 aircraft.

The pictures of the model, shown in Figure 6, were obtained from LS-POST [13], the post-processing software for LS-DYNA. A figure depicting the location of the point elements is shown in Figure 7. Point elements were used to assign concentrated masses representing the seats, ATDs, mannequins, luggage, fuel, and other ballast to nodes in the model. The inertial properties of the tail section were represented as a single concentrated mass, which was positioned at the approximate CG location of the tail section. The concentrated mass was connected to the aircraft model through beam elements, as shown in Figure 6(b). This representation was necessary since data defining the geometry and dimensions of the tail section were not provided. This approximation of the tail section is appropriate since a detailed finite element model of the tail section is not important to the overall simulation. A separate NASTRAN [14] analysis was performed to determine the distribution of nodal masses to represent the fuel in the wing. In this analysis, solid elements were defined by the upper and

lower wing skins, with one element thickness between each skin. The nodes on the bottom skin were fixed. The solid elements were assigned properties with the density of water, and a gravitational loading was applied. The resulting constraint forces on the bottom nodes were converted into concentrated masses at each node. Once this analysis was completed, the concentrated masses determined from the NASTRAN analysis were copied into the LS-DYNA model.

Table 1. Material properties used in the model.

Material type	Young's modulus (E)		Poisson ratio (μ)	Density (ρ)		Yield stress (σ_Y)		Hardening modulus (E_H)		Failure strain (ϵ_{ult}), %
	psi	GPa		lb-s ² /in ⁴	g/cm ³	ksi	Mpa	ksi	MPa	
Al-2024-T3	9.62e06	66.33	.33	2.59e-4	2.76	35.25	243.0	119.9	826.7	14.63
Al-7075-T6	1.03e07	71.02	.33	2.61e-4	2.794	52.22	360.0	145.3	1001.8	4.49
Al-7050-T7452	1.04e07	71.71	.33	2.64e-4	2.822	60.0	413.7	145.3	1001.8	3.5
Ti-6Al-4V	1.71e07	117.9	.31	4.24e-4	4.536	125.0	861.9	203.0	1399.7	8.0

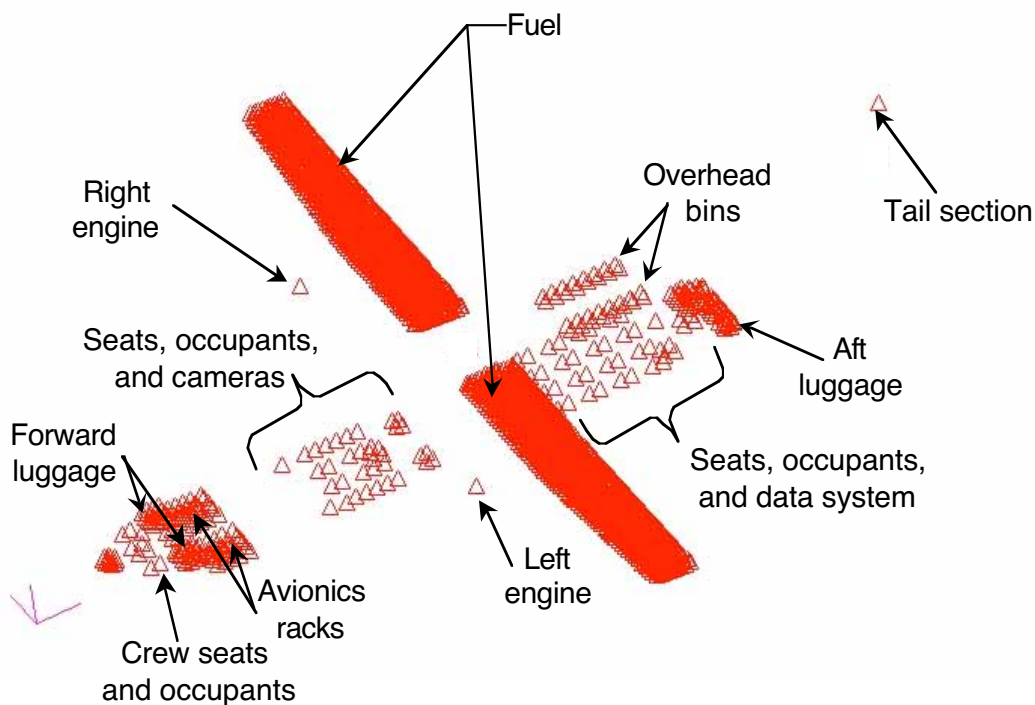


Figure 7. The location of point elements in the model.

All of the nodes in the aircraft model were given an initial velocity of -360 in/s (-9.14 m/s). For the impact surface, all of the edge nodes were constrained from translational and rotational motion. The model was executed in LS-DYNA (version 970) for 0.25 seconds of simulation time, which required 93 hours of CPU time on a single processor Hewlett Packard workstation x4000.

As a quality check on the model, the total weight and longitudinal CG location of the model were compared with those of the test article. The weight of the full-loaded and instrumented aircraft prior to the test was 33,200 lb. (15,060 kg) and the total weight of the aircraft model was 33,120 lb. (15,023 kg), just 80 lb. (36.3 kg) lighter than the test article. The measured longitudinal CG position of the test article was 469.2 in. (11.92 m) from the reference location. For the model, the longitudinal CG position was 471.5 in. (11.98 m) from the reference location, less than 3 inches (.076 m) from the experimental value.

TEST-ANALYSIS CORRELATION

The test-analysis correlation consists of comparisons of experimental and analytical structural deformation and selected acceleration and velocity time-history responses.

Comparison of Structural Deformation

Comparisons of test article and model deformations are shown in Figure 8 from 0.05 to 0.25-seconds in .05-second intervals. The pictures of model deformation were obtained from the post-processing file, and the experimental pictures were captured from the high-speed film. In general, the model accurately predicts the structural deformation and failure behavior of the test article, including collapse and failure of the fuselage structure beneath the wing. In the experiment, structural failure is initiated by fracture of the fuselage frames at FS 25 and FS 27, and is not caused by failure of the “dog bone” beams. The same failure behavior is observed in the model, as shown in Figure 9. This figure shows the predicted deformation of the fuselage frames at FS 25 and FS 27, along with the “dog bone” beams and the wing attachments, at the beginning and end of the simulation. In the model, the frames are highly deformed and fractured, while the “dog bone” beams remain intact. Note that in LS-DYNA, failed elements are removed from the model. The frame failures allow the wing to translate downward through the fuselage cabin. In addition to the vertical translation, the wing tips in the model also exhibit significant vertical deflection due to elastic bending of the wing. In the test, some oscillatory bending of the wing is observed; however, the tip displacement is considerably less than in the model. The wing also begins to rotate forward immediately following impact, due to the forward placement of the simulated engines. However, this behavior is not captured by the model.

Comparison of Selected Time-History Responses

The raw experimental acceleration data were plotted versus time, integrated to obtain the velocity time-history responses, and filtered using a low-pass digital filter based on the SAE J211/1 specifications [15]. A variety of cut-off frequencies were applied in an attempt to obtain a well-defined acceleration pulse, while at the same time not distorting the integrated velocity response. Distortion in the velocity response is determined by comparing the velocity time-histories obtained by integrating the raw and filtered experimental acceleration data. A low-pass cut-off frequency of 33.2 Hz was selected because it generally met these criteria. All of the experimental and analytical acceleration time-histories shown in the paper are filtered using this cut-off frequency. Also, since minimal distortion was evident, the experimental and analytical velocity responses shown in the paper were obtained by integrating the filtered acceleration data.











Time, s	Test article	LS-DYNA simulation
0.05		
0.10		
0.15		
0.20		
0.25		

Figure 8. Comparison of structural deformation.

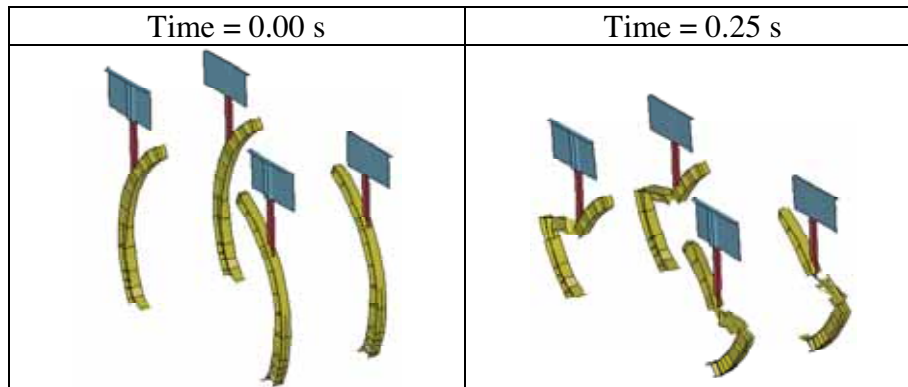


Figure 9. Predicted deformation of the fuselage frames (FS 25 and FS 27) that support the wing at times 0.00 and 0.25-seconds.

The experimental and analytical acceleration and velocity responses of the left outer seat track at FS 20 are shown in Figure 10. For the test, the acceleration response exhibits two main peaks, as indicated in Figure 10 (a). The first acceleration peak (18-g) is smaller in magnitude than the second (28-g). At this location, the predicted acceleration response also exhibits two peaks; however, the first peak is higher in magnitude (28-g) than the second (17-g). The filtered experimental and analytical acceleration data were integrated to obtain the velocity responses plotted in Figure 10 (b). Both curves are closely matched up to 0.06 seconds. After that time, the analytical velocity response crosses zero velocity at 0.075 seconds and exhibits a rebound of

about 34 in/s (0.86 m/s). Whereas, the experimental response flattens out after 0.06 seconds and does not cross zero until 0.15 seconds. The maximum rebound velocity exhibited by the experimental response is 30 in/s (0.76 m/s).

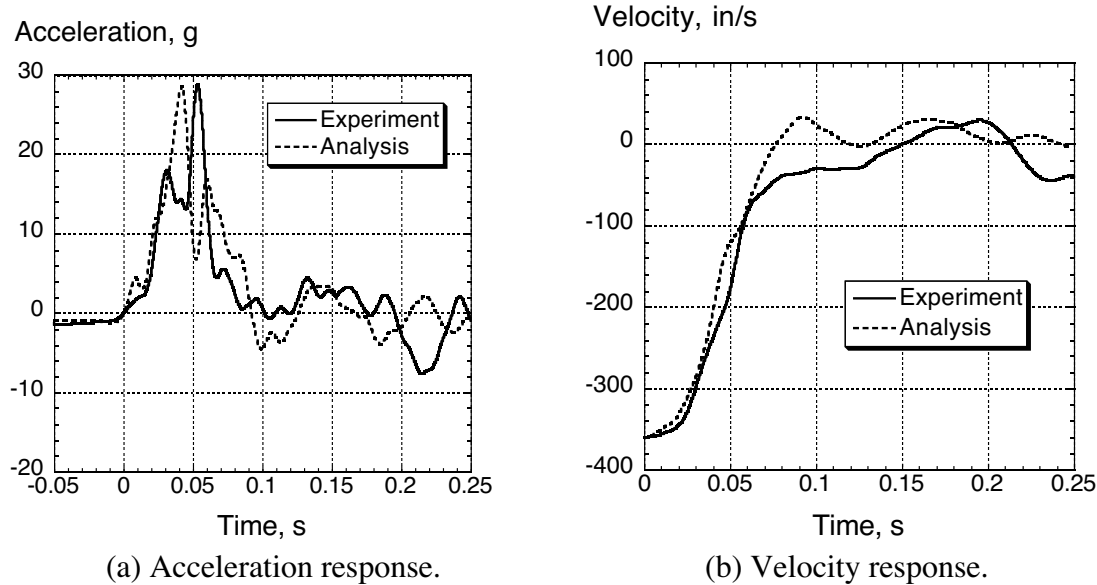


Figure 10. Time-history responses for the left outer seat track at FS 20.

The experimental and analytical acceleration and velocity responses of the right outer seat track at FS 18 are shown in Figure 11. For this location, the peak acceleration values for the test and analysis are of the same magnitude, about 24-g. Also, the predicted velocity response closely matches the experimental response, i.e. both curves cross zero velocity at the same time (.08 seconds), though the experimental response exhibits a slightly higher rebound velocity of 50 in/s (1.27 m/s).

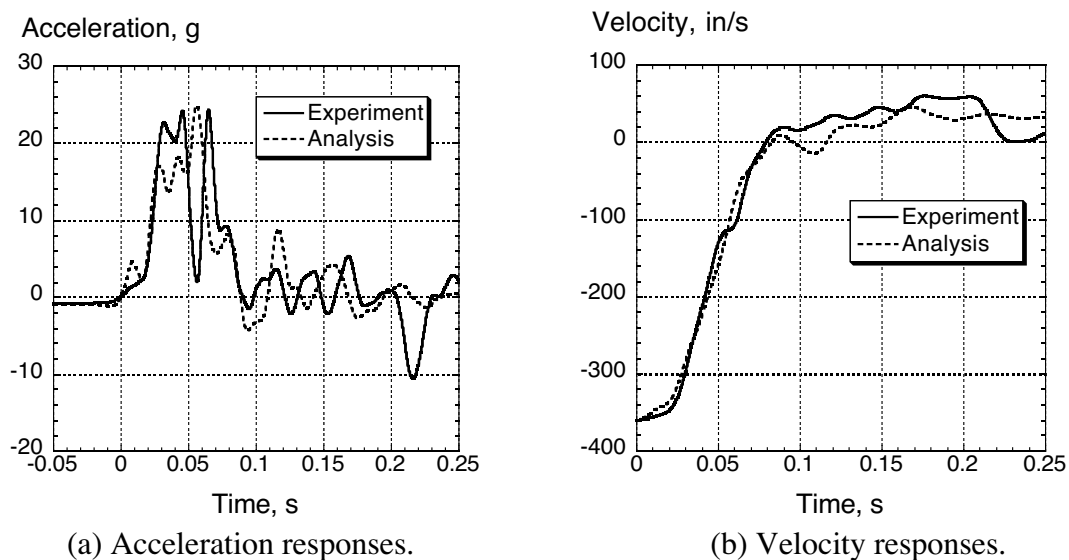


Figure 11. Time-history responses for the right outer seat track at FS 18.

Next, the experimental and analytical acceleration and velocity responses of the right side of the cockpit floor are plotted in Figure 12. Again, the experimental acceleration response exhibits two peaks; however, in this case the first peak (34-g) is higher in magnitude than the second (28-g). The predicted peak acceleration is 26-g. The experimental pulse is shorter in duration than the analytical response by about 0.02 seconds, as indicated in the velocity plot of Figure 12 (b). However, both curves exhibit the same rebound velocity of 90 in/s (2.29 m/s).

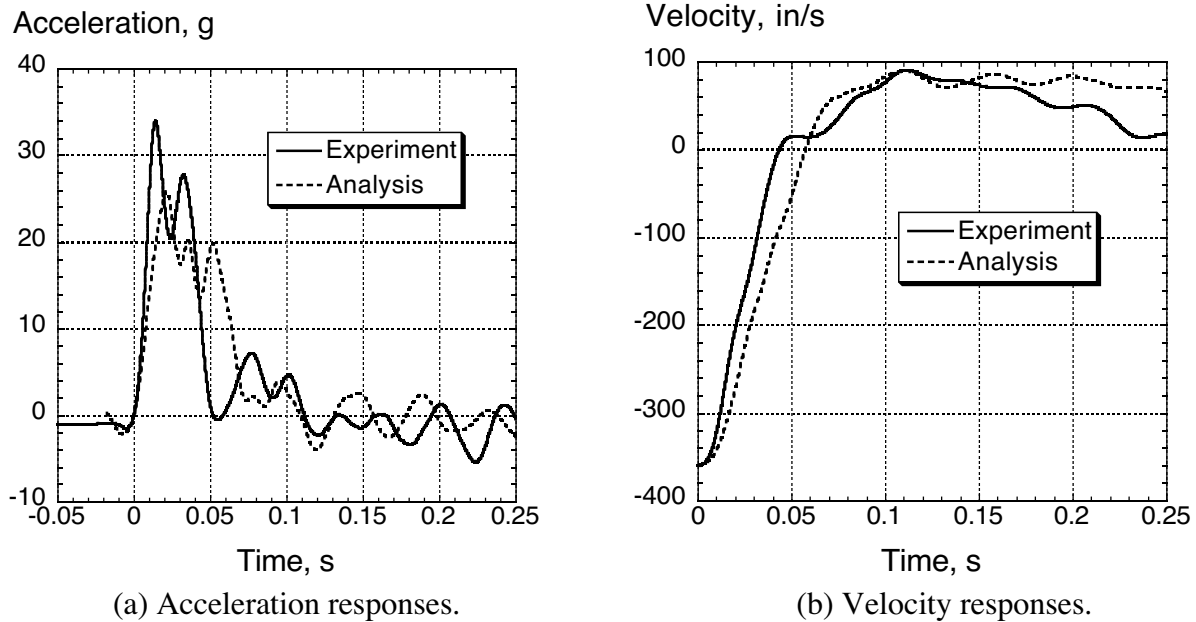
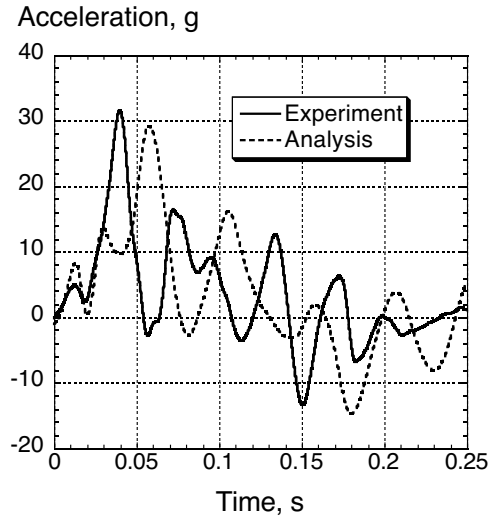
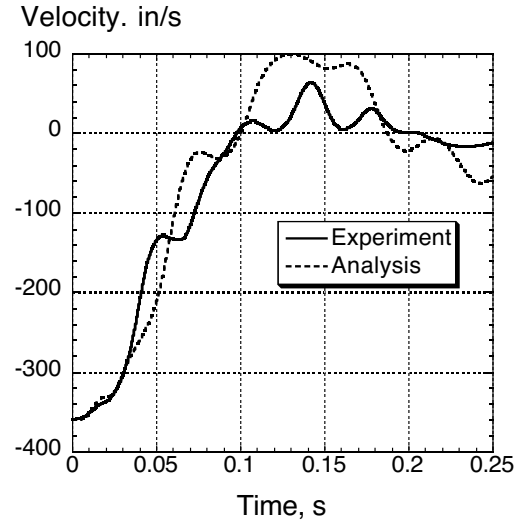


Figure 12. Time-history responses of the right side of the cockpit floor.

The experimental and analytical acceleration and velocity responses of the left inner seat track at FS 29 and the right inner seat track at FS 35 are plotted in Figures 13 and 14, respectively. The locations of these accelerometers are shown in the schematic drawing of Figure 2. The accelerometer at FS 29 is located on the floor slightly to the rear of the fuselage frames supporting the wings, while the accelerometer at FS 35 is located on the floor at the very rear of the aircraft. At these two locations, the filtered experimental acceleration responses exhibit high-amplitude, low frequency responses, making it difficult to discern a well-defined acceleration pulse. In general, the predicted acceleration responses match the peak values and the pulse durations of the experimental acceleration responses at these two locations. However, the comparison of the velocity responses is, perhaps, a better measure of the level of correlation, as shown in Figures 13(b) and 14(b).



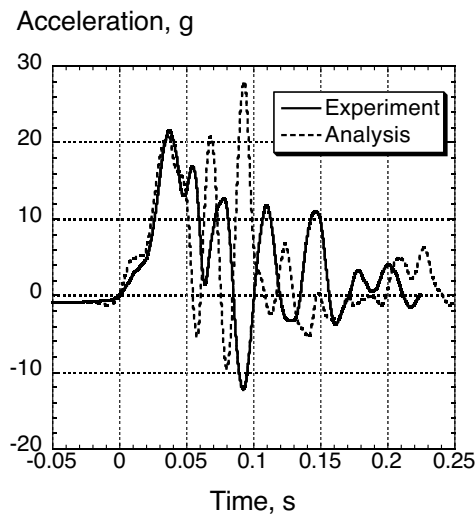
(a) Acceleration responses.



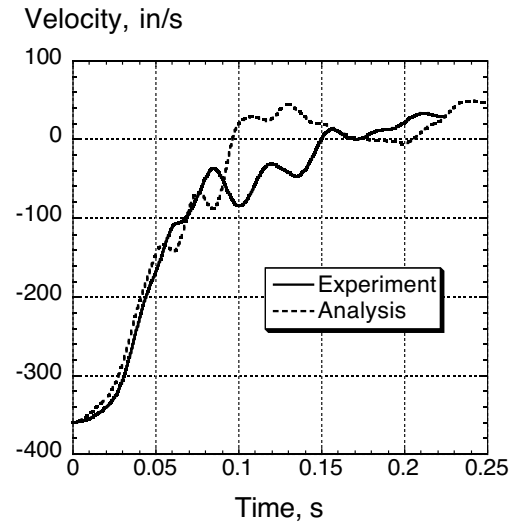
(b) Velocity responses.

Figure 13. Time-history responses of the left inner seat track at FS 29.

The experimental and predicted acceleration and velocity responses of the center of the tail section at FS 47 are plotted in Figure 15. Unlike the floor acceleration responses, most of which had pulse durations of 0.1 second or less, this response is 0.2 seconds in duration. Both the experimental and analytical acceleration responses exhibit a single pulse, of approximately the same duration and magnitude. The experimental and analytical velocity responses, shown in Figure 15 (b), show nearly perfect agreement, with both curves crossing zero velocity at nearly the same time (0.16 seconds) and exhibiting a maximum rebound velocity of 147 in/s (3.73 m/s) at 0.21 second.



(a) Acceleration responses.



(b) Velocity responses.

Figure 14. Time-history responses of the right inner seat track at FS 35.

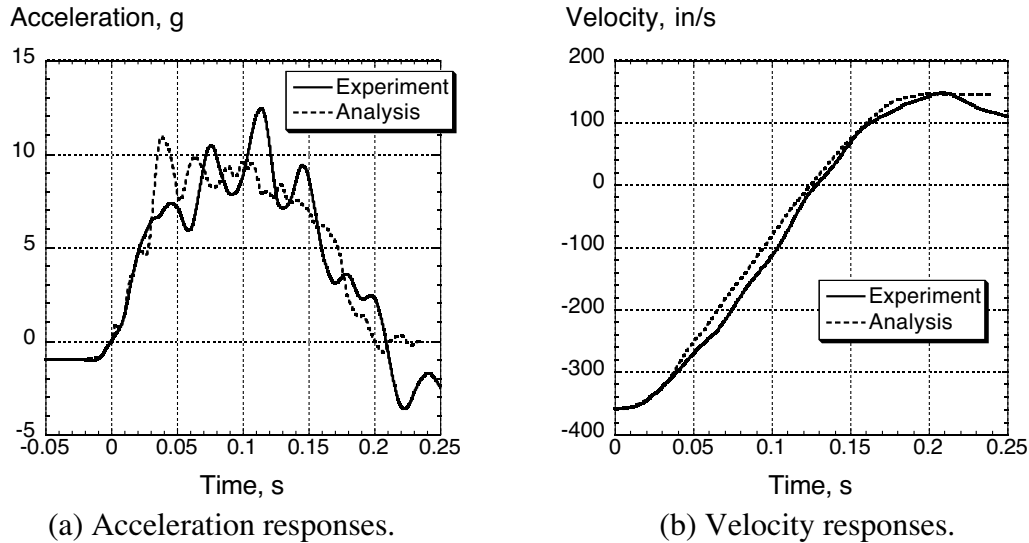


Figure 15. Time-history responses of the center tail section at FS 47.

The experimental and analytical acceleration and velocity responses of the left sidewall at FS 18 are plotted in Figure 16. This accelerometer was located on the sidewall approximately 12 in. (0.305 m) above the floor and was oriented in the vertical direction. The analytical acceleration response closely matches the magnitude (peak acceleration of 26.5 g's for the analysis compared with 22.5 g's for the experiment) of the experimental pulse. The velocity responses, shown in Figure 16 (b), are close up to 0.075 seconds, after which time the analytical curve crosses zero velocity at 0.08 seconds and exhibits a maximum rebound velocity of 36 in/s (0.91 m/s). However, the experimental response flattens out and does not cross zero velocity until 0.12 seconds, after which it exhibits a prolonged rebound velocity of 60 in/s (1.52 m/s), not seen in the analytical curve.

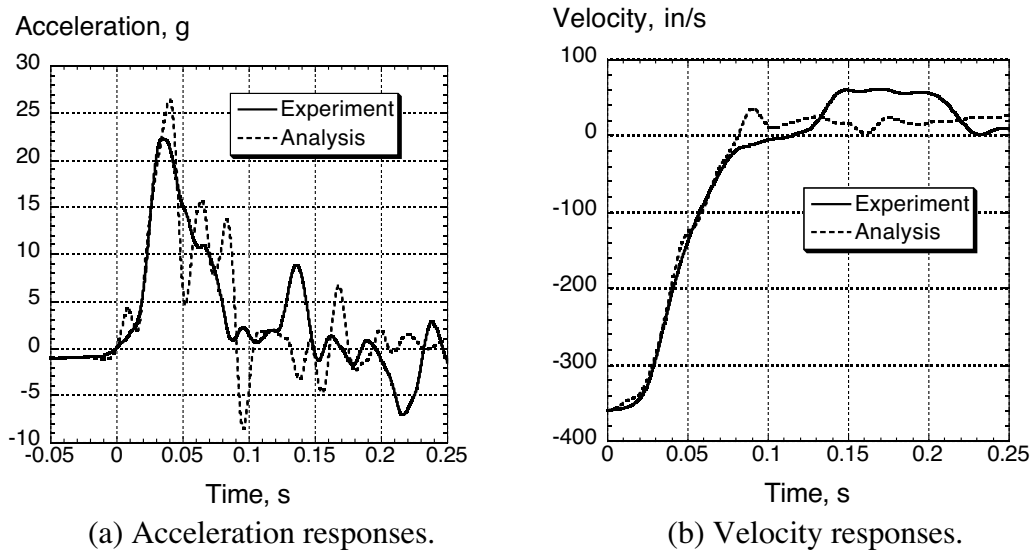


Figure 16. Time-history responses of the left sidewall at FS 18.

The final time-history comparison is shown in Figure 17, in which the experimental and analytical acceleration and velocity responses of the center ceiling at FS 26 are plotted. The position of this accelerometer is at the center of the bottom skin of the wing. The filtered experimental and analytical acceleration data contain high-amplitude, low frequency responses, as seen in Figure 17(a). The predicted acceleration response overshoots the magnitude of the initial peak acceleration of the experimental response; however, it accurately captures the dip and subsequent rise in the experimental response that occurs at approximately 0.1 seconds. At this accelerometer location, the analytical response appears to be reducing velocity more quickly than the experiment, as shown in Figure 17 (b). For example, at 0.04 seconds, the experimental velocity is -289 in/s (7.34 m/s), while the predicted velocity is -204 in/s (5.18 m/s). Also, note that neither response has crossed zero velocity by 0.25 seconds indicating that the wing is still translating downward.

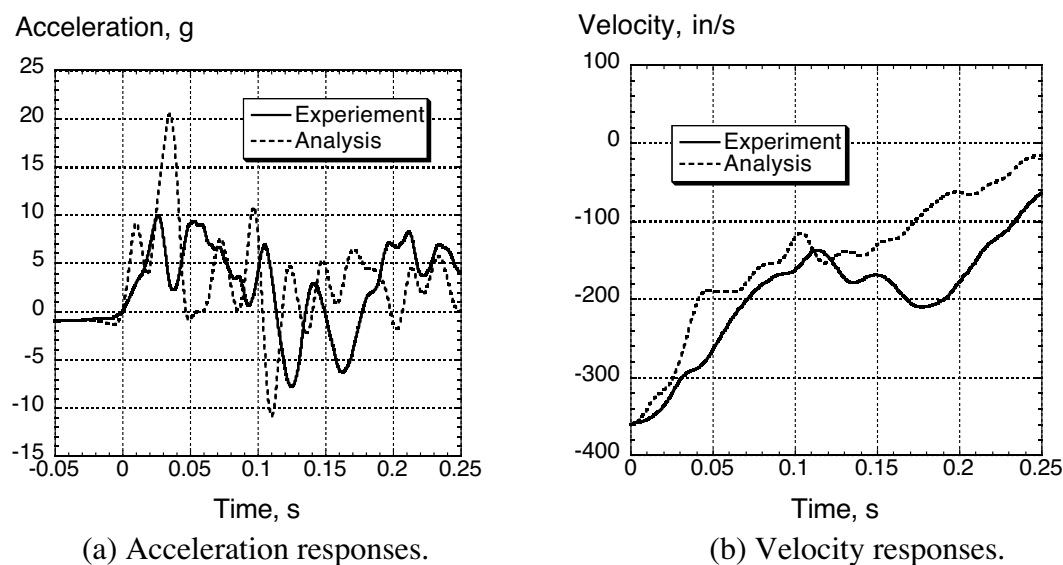


Figure 17. Experimental and analytical time-history responses of the ceiling at FS 26.

DISCUSSION OF RESEULTS

In general, a high level of agreement was obtained between the experimental and analytical data, especially when considering the complexity of the test article. The simulation accurately predicted the major structural failure, the collapse and failure of the fuselage frames supporting the wing structure. However, some differences in the experimental and analytical structural deformations were observed. In the model, the wing exhibited more bending than seen experimentally, resulting in higher wing tip displacement. Also, in the test, the wing exhibits a large forward rotation due to the presence of the simulated engine masses. While the inertial properties of the simulated engines were represented in the model using concentrated masses, the model did not capture this forward rotation of the wing. These differences indicate that the material properties and/or average dimensions used to represent the wing model should be modified to increase the structural stiffness of the wing to better match the response of the test article.

The model predicted the experimental acceleration and velocity time-histories quite well. The high level of agreement achieved for the floor-level acceleration responses is important in that these pulses are transmitted to the seats and occupants during a crash. Also, these data are needed to accurately assess dynamic seat criteria for commuter-class aircraft.

CONCLUDING REMARKS

A full-scale three-dimensional finite element model of a twin-turboprop high-wing commuter-class aircraft, the ATR42-300, was developed and executed as a crash simulation. The analytical predictions were correlated with test data obtained from a 30-ft/s (9.14 m/s) vertical drop test of the aircraft that was conducted using the Dynamic Drop Test Facility at the FAA William J. Hughes Technical Center in Atlantic City, NJ. For the test, the aircraft was configured with seats, anthropomorphic test dummies, luggage in the forward and aft compartments, and 8,700-lb. (3,946 kg) of water in the wings to represent the fuel loading. The finite element model of the aircraft was developed from direct measurements of the airframe geometry and contained 57,643 nodes and 62,979 elements including 60,197 quadrilateral shell elements; 551 triangular shell elements; 526 beam elements; and, 1,705 point elements. The model was executed in LS-DYNA, a commercial code for performing explicit transient dynamic simulations.

The analytical predictions correctly simulated the major damage mode seen during the test, which was collapse and failure of the fuselage structure beneath the wing. These structural failures allowed the wing to displace vertically through the fuselage cabin. In general, a high level of agreement was obtained between the experimental and analytical data, especially when considering the complexity of the test article. It was particularly important to obtain accurate prediction of the floor-level acceleration responses, since these pulses are transmitted to the seat and occupants. These data will be useful in evaluating the FAA's proposed dynamic seat standards for commuter-class aircraft.

ACKNOWLEDGEMENTS

The authors acknowledge Gary Frings, Allan Abramowitz, Tong Vu, and Tim Smith of the FAA for their assistance with the model geometry development, and for providing the test data, pre- and post-test photographs, and videos of the test. Also, we acknowledge the support of Alan Stockwell and Hasan Abu-Khajeel of Lockheed Martin Space Operations at NASA Langley Research Center for their assistance with model discretization and the NASTRAN analysis.

REFERENCES

1. Noor, A., and Carden H. C., editors, "Computational Methods for Crashworthiness," NASA Conference Publication 3223, October 1993.
2. Abramowitz, A., Smith, T. G, Vu, T., "Vertical Drop Test of a Narrow-Body Transport Section with a Conformable Auxiliary Fuel Tank Onboard." DOT/FAA/AR-00/56, October 2000.

3. Abramowitz, A., Smith, T. G., Vu, T., Zvanya, J. R., "Vertical Drop Test of a Narrow-Body Transport Fuselage Section with Overhead Stowage Bins," DOT/FAA/AR-01/100, September 2002.
4. Anon., "MSC.Dytran User's Manual Version 4.7," The MacNeal-Schwendler Corporation, Los Angeles, CA, 1999.
5. Jackson, K. E. and Fasanella, E. L., "Crash Simulation of a Vertical Drop Test of a B737 Fuselage Section with Overhead Bins and Luggage," Proceedings of the Third Triennial Aircraft Fire and Cabin Safety Conference, Atlantic City, NJ, October 22-25, 2001.
6. Fasanella, E. L. and Jackson, K. E., "Crash Simulation of a Vertical Drop Test of a B737 Fuselage Section with an Auxiliary Fuel Tank," Proceedings of the Third Triennial Aircraft Fire and Cabin Safety Conference, Atlantic City, NJ, October 22-25, 2001.
7. Jackson, Karen E. and Fasanella, E. L., "Crash Simulation of Vertical Drop Tests of Two Boeing 737 Fuselage Sections," DOT/FAA/AR-02/62, August 2002.
8. Anon., "MSC.PATRAN," Publication No. 903077, Version 6, The MacNeal-Schwendler Corporation, 1996.
9. Anon., "LS-DYNA Keyword User's Manual," Version 970, Livermore Software Technology Company, Livermore, CA, April 2003.
10. Anon., "Weight and Balance Manual," Avions de Transport Regional, Service Bulletin No. ATR42-34-0114, issued March 1992.
11. Jackson, K. E., and Fasanella, E. L., "Development of an LS-DYNA Model of an ATR42-300 Aircraft for Crash Simulation" Proceedings of the Eighth International LS-DYNA Users Conference, May 2-4, 2004 in Dearborn, MI.
12. Military Handbook 5H, U.S. Department of Defense, 1 December 1998.
13. Anon., "LS-PRE/POST v. 1.0 Manual" Livermore Software Technology Company, Livermore, CA, August 27, 2002.
14. Anon., "MSC/NASTRAN Quick Reference Guide," Version 70.5, The MacNeal-Schwendler Corporation, Los Angeles, CA, February 1998.
15. Society of Automotive Engineers, Recommended Practice: Instrumentation for Impact Test – Part 1, Electronic Instrumentation, SAE J211/1, March 1995.